

# Improving CACC Robustness to Parametric Uncertainty via Plant Equivalent Controller Realizations

Mischa Huisman, Thomas Arnold, Erjen Lefeber, Nathan van de Wouw, and Carlos Murguia.

**Abstract**—Cooperative Adaptive Cruise Control (CACC) enables vehicle platooning through inter-vehicle communication, improving traffic efficiency and safety. Conventional CACC relies on feedback linearization, assuming exact vehicle parameters; however, longitudinal vehicle dynamics are nonlinear and subject to parametric uncertainty. Applying feedback linearization with a nominal model yields imperfect cancellation, leading to model mismatch and degraded performance with off-the-shelf CACC controllers. To improve robustness without redesigning the CACC law, we explicitly model the mismatch between the ideal closed-loop dynamics assumed by the CACC design and the actual dynamics under parametric uncertainties. Robustness is formulated as an  $\mathcal{L}_2$  trajectory-matching problem, minimizing the energy of this mismatch to make the uncertain system behave as closely as possible to the ideal model. This objective is addressed by optimizing over plant equivalent controller (PEC) realizations that preserve the nominal closed-loop behavior while mitigating the effects of parametric uncertainty. Stability and performance are enforced via linear matrix inequalities, yielding a convex optimization problem applicable to heterogeneous platoons. Experimental results demonstrate improved robustness and performance under parametric uncertainty while preserving nominal CACC behavior.

## I. INTRODUCTION

Cooperative Adaptive Cruise Control (CACC) is a well-explored technology for improving traffic throughput, fuel efficiency, and safety in intelligent transportation systems. Enabling CACC through Vehicle-to-Vehicle communication allows vehicles to form platoons and closely follow one another while maintaining string stability [1].

Many CACC designs, as well as other longitudinal controllers, rely on an additional nonlinear control layer that performs feedback linearization of the vehicle dynamics to facilitate controller design and analysis [2–6]. However, feedback linearization inherently assumes exact knowledge of vehicle and road parameters, such as mass, aerodynamic drag, viscous friction, and driveline dynamics. In practice, these parameters are uncertain and may vary significantly over time, for instance, due to changing payload conditions in heavy-duty vehicles,

The research leading to these results has received funding from the European Union’s Horizon Europe programme under grant agreement No 101069748 – SELFY project.

M. Huisman, T. Arnold, C. Murguia, E. Lefeber, and N. van de Wouw are with the Department of Mechanical Engineering, Eindhoven University of Technology, The Netherlands. [M.R.Huisman, C.G.Murguia, A.A.J.Lefeber, N.v.d.Wouw]@tue.nl

C. Murguia is with the Department of Engineering Systems and Design, Singapore University of Technology and Design, Singapore. murguia\_rendon@sutd.edu.sg

which can lead to instability and performance degradation if not accounted for.

To address model uncertainty in platoons, a variety of robust and adaptive control strategies have been proposed in the literature. Extensive research has focused on uncertainty in driveline dynamics, including online driveline parameter estimation [7], robust  $\mathcal{H}_\infty$  control methods [8, 9], and self-learning techniques [10]. Other approaches consider additional sources of uncertainty, such as wind gusts, which are addressed using robust model predictive control in [11]. Nonlinear adaptive CACC schemes with online parameter updates have also been investigated [12], although such methods may be sensitive to measurement noise. Furthermore, adaptive control strategies that account for uncertain communication and actuation delays are proposed in [5, 13].

Despite these advances, the existing approaches typically focus on specific subsets of uncertainty or rely on simplified vehicle models, even though nonlinear dynamics and their uncertainties play an important role in, e.g., safety-critical scenarios [14]. Therefore, this paper first introduces a general nonlinear longitudinal vehicle model that explicitly accounts for multiple resistive forces, following established modeling approaches [14–17]. Feedback linearization is then applied without assuming exact knowledge of all model parameters, allowing uncertainty not only in driveline dynamics or wind velocity, but also in vehicle mass, effective mass, and aerodynamic drag and viscous friction coefficients.

To enhance the robustness and performance of the closed-loop system in the presence of parametric model uncertainty, we exploit plant equivalent (PEC) realizations [18, 19]. We leverage degrees of freedom in the realization of a given dynamic CACC scheme, referred to herein as the base controller, to mitigate the impact of uncertainty without altering the desired nominal performance. By appropriately selecting the PEC realization, the propagation of parametric uncertainty through the closed-loop dynamics can be mitigated. By defining nominal and uncertainty-induced error states, the proposed framework enables systematic tuning of the controller realization to minimize both transient and steady-state performance degradation, while guaranteeing stability.

The resulting closed-loop system is formulated as a polytopic uncertain linear system, where the PEC realization design variables enter linearly. This structure allows robust stability and performance to be enforced through a set of linear matrix inequalities evaluated at

the vertices of the uncertainty polytope. The design objective combines the minimization of the average output energy induced by uncertainty with bounds on the worst-case input-output gain (i.e.,  $\mathcal{H}_\infty$ ), yielding a convex optimization problem that can be efficiently solved using SDP solvers. The proposed PEC realizations apply to heterogeneous platoons, while explicitly optimizing performance with respect to model uncertainty. The proposed method is experimentally validated on a vehicle, demonstrating improved robustness under uncertainty.

The remainder of this paper is organized as follows. Section II introduces the required preliminaries. Section III presents the nonlinear vehicle model and introduces the PEC realizations. Section IV describes the framework for robust stability and performance optimization using PEC realizations. Section V compares simulation and experimental results, and Section VI concludes the paper.

## II. Mathematical Preliminaries

The symbol  $\mathbb{R}$  stands for the real numbers,  $\mathbb{R}_{>0}$  ( $\mathbb{R}_{\geq 0}$ ) denotes the set of positive (non-negative) real numbers. The symbol  $\mathbb{N}$  denotes the set of natural numbers, including zero. The  $n \times m$  matrix composed of only zeros is denoted by  $0_{n \times m}$ , or 0 when its dimension is clear. The notation  $A \succeq 0$  (resp.,  $A \preceq 0$ ) indicates that the matrix  $A$  is positive (resp., negative) semidefinite, i.e., all the eigenvalues of the symmetric matrix  $A$  are positive (resp., negative) or equal to zero, whereas  $A \succ 0$  (resp.,  $(A \prec 0)$ ) indicates the positive (resp., negative) definiteness, i.e., all the eigenvalues are strictly positive (resp., negative). Time dependencies of signals are often omitted for simplicity of notation.

**Definition 1** (Polytopic uncertain system [20, 21]) Consider the linear system with model uncertainties

$$\dot{x}(t) = A(\Delta)x(t) + B(\Delta)u(t), \quad (1a)$$

$$y(t) = C(\Delta)x(t) + D(\Delta)u(t), \quad (1b)$$

where  $x(t) \in \mathbb{R}^n$  is the state,  $u(t) \in \mathbb{R}^m$  is the input, and  $y(t) \in \mathbb{R}^r$  is the output. For a polytopic uncertain system, matrices  $A(\Delta)$ ,  $B(\Delta)$ ,  $C(\Delta)$ , and  $D(\Delta)$  are subject to parametric uncertainty and belong to a convex polytope  $\Omega := \text{conv}\{S^{[1]}, S^{[2]}, \dots, S^{[N]}\}$ , where each vertex  $S^{[k]}$  is defined as a tuple

$$S^{[k]} := (A^{[k]}, B^{[k]}, C^{[k]}, D^{[k]}), \quad k = 1, \dots, N. \quad (2)$$

Accordingly, for any admissible uncertainty  $\Delta$ , the system matrices admit the representation

$$\Omega = \sum_{k=1}^N \alpha_k S^{[k]}, \quad \sum_{k=1}^N \alpha_k = 1, \quad \alpha_k \geq 0, \quad k = 1, \dots, N. \quad (3)$$

**Lemma 1** (Quadratic Stability [20, 21]) Consider the polytopic system described in Definition 1 with  $u(t) = 0$ . If there exists a matrix  $P \in \mathbb{R}^{n \times n}$  such that  $P \succ 0$  and

$$(A^{[k]})^\top P + PA^{[k]} \prec 0, \quad \forall k \in \{1, \dots, N\}, \quad (4)$$

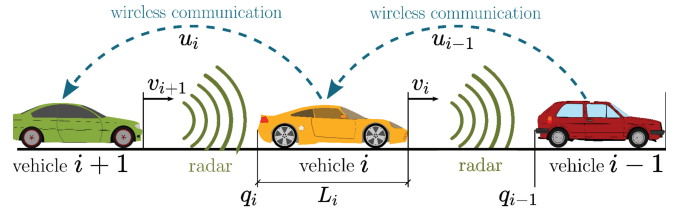


Fig. 1. CACC-equipped string of vehicles.

then the origin of the system is asymptotically stable for all admissible uncertainties  $\Delta$ .

**Lemma 2** (Bounded Real Lemma [20, 21]) Consider the polytopic system in Definition 1 with performance output  $z(t) = C_z(\Delta)x(t)$ . If there exists a symmetric matrix  $P \succ 0$  and a scalar  $\gamma > 0$  such that, for all vertices  $k = 1, \dots, N$ ,

$$\begin{bmatrix} (A^{[k]})^\top P + PA^{[k]} + (C_z^{[k]})^\top C_z^{[k]} & PB^{[k]} \\ (B^{[k]})^\top P & -\gamma I \end{bmatrix} \preceq 0, \quad (5)$$

then the  $\mathcal{L}_2$ -gain from  $u$  to  $z$  satisfies  $\|z\|_{\mathcal{L}_2} \leq \sqrt{\gamma}\|u\|_{\mathcal{L}_2}$ , for all admissible uncertainties  $\Delta$  and all  $u \in \mathcal{L}_2$ .

## III. Problem Setting

Consider a platoon of  $m$  vehicles, schematically depicted in Fig. 1, indexed by  $i \in S_m := \{1, \dots, m\}$ , where  $i = 1$  denotes the lead vehicle. The longitudinal dynamics of the  $i$ th vehicle are commonly modeled as [14–17]

$$\dot{F}_{\text{drive},i} = -\frac{F_{\text{drive},i}}{\tau_i} + \frac{\eta_i}{\tau_i}, \quad (6a)$$

$$m_{\text{eff},i} a_i = F_{\text{drive},i} - F_{\text{d},i} - F_{\text{v},i} - F_{\text{r},i} - F_{\text{g},i}, \quad (6b)$$

where  $m_{\text{eff},i}$  denotes the effective vehicle mass,  $\tau_i$  the driveline time constant,  $F_{\text{drive},i}$  the driving force,  $\eta_i$  the engine input, and  $a_i$  the acceleration of vehicle  $i$ . The resistive forces consist of aerodynamic drag  $F_{\text{d},i}$ , viscous friction  $F_{\text{v},i}$ , rolling resistance  $F_{\text{r},i}$ , and the gravitational component  $F_{\text{g},i}$  of vehicle  $i$ , which are defined as

$$F_{\text{d},i} = C_{\text{d},i}(v_i - v_w)^2, \quad F_{\text{v},i} = f_{\text{v},i} v_i, \quad (6c)$$

$$F_{\text{r},i} \approx f_{\text{r},i} m_i g, \quad F_{\text{g},i} \approx m_i g \alpha_i, \quad (6d)$$

with  $v_i$  the vehicle velocity,  $C_{\text{d},i}$  the drag coefficient,  $v_w$  the wind speed,  $f_{\text{v},i}$  the viscous friction coefficient,  $f_{\text{r},i}$  the rolling resistance coefficient,  $m_i$  the vehicle mass,  $g$  the gravitational constant, and  $\alpha_i$  the road slope.

Assuming small road slopes  $\alpha_i$ , and slowly varying rolling and gravitational forces, differentiation of (6b) together with (6c) yields the nonlinear acceleration dynamics

$$\dot{a}_i = -\frac{f_{\text{v},i} - 2C_{\text{d},i}v_w}{\tau_i m_{\text{eff},i}} v_i - \left( \frac{f_{\text{v},i} - 2C_{\text{d},i}v_w}{m_{\text{eff},i}} + \frac{1}{\tau_i} \right) a_i - \frac{C_{\text{d},i}}{\tau_i m_{\text{eff},i}} v_i^2 - \frac{2C_{\text{d},i}}{m_{\text{eff},i}} v_i a_i - \frac{m_i(f_{\text{r},i}g + g\alpha_i) + C_{\text{d},i}v_w^2}{\tau_i m_{\text{eff},i}} + \frac{1}{\tau_i m_{\text{eff},i}} \eta_i. \quad (7)$$

The control objective for each follower vehicle is to keep a desired inter-vehicle distance  $d_{\text{r},i} = r_i + h_i v_i$ ,  $i \in S_m \setminus \{1\}$ , with time gap  $h_i > 0$  and standstill distance  $r_i \geq 0$ . Several CACC schemes have been proposed in the literature to achieve this objective, e.g., [3–5],

which are based on a vehicle model obtained via feedback linearization of (7).

Feedback linearization is achieved via engine input  $\eta_i$ , and requires exact knowledge of all parameters in (7). Since this assumption is generally unrealistic, we introduce six parameter groups  $p_j$ ,  $j \in \{1, \dots, 6\}$ , each characterized by a nominal estimate  $p_{j|0}$  and an additive uncertainty  $\Delta_j$ . This allows rewriting (7) as

$$\begin{aligned}\dot{a}_i = & -(p_{1|0} + \Delta_1)v_i - (p_{2|0} + \Delta_2)a_i - (p_{3|0} + \Delta_3)v_i^2 \\ & - (p_{4|0} + \Delta_4)v_i a_i - (p_{5|0} + \Delta_5) + (p_{6|0} + \Delta_6)\eta_i.\end{aligned}\quad (8)$$

Following [3, 4], the desired vehicle model is defined as

$$\dot{q}_i = v_i, \quad \dot{v}_i = a_i, \quad (9a)$$

$$\dot{a}_i = -\frac{1}{\tau_{\text{des},i}}a_i + \frac{1}{\tau_{\text{des},i}}u_i, \quad (9b)$$

with position  $q_i$ , velocity  $v_i$ , new input  $u_i$  and design parameter  $\tau_{\text{des},i} > 0$ . Using the nominal parameter estimates  $p_{j|0}$ , the feedback linearizing control law yields

$$\begin{aligned}\eta_i = & p_{6|0}^{-1} \left( p_{1|0}v_i + \left( p_{2|0} - \frac{1}{\tau_{\text{des},i}} \right) a_i + p_{3|0}v_i^2 \right. \\ & \left. + p_{4|0}v_i a_i + p_{5|0} + \frac{1}{\tau_{\text{des},i}}u_i \right).\end{aligned}\quad (10)$$

Substituting (10) into (8) yields the perturbed dynamics

$$\dot{a}_i = -\frac{1}{\tau_{\text{des},i}}a_i + \frac{1}{\tau_{\text{des},i}}u_i + \phi_i, \quad (11a)$$

$$\begin{aligned}\phi_i = & \theta_{i,1}v_i + \theta_{i,2}a_i + \theta_{i,3}v_i^2 + \theta_{i,4}v_i a_i \\ & + \theta_{i,5} + \theta_{i,6}u_i,\end{aligned}\quad (11b)$$

with

$$\theta_{i,1} = \frac{p_{1|0}}{p_{6|0}}\Delta_6 - \Delta_1, \quad (11c)$$

$$\theta_{i,2} = \left( \frac{p_{2|0}}{p_{6|0}} - \frac{1}{p_{6|0}\tau_{\text{des},i}} \right) \Delta_6 - \Delta_2, \quad (11d)$$

$$\theta_{i,3} = \frac{p_{3|0}}{p_{6|0}}\Delta_6 - \Delta_3, \quad \theta_{i,4} = \frac{p_{4|0}}{p_{6|0}}\Delta_6 - \Delta_4, \quad (11e)$$

$$\theta_{i,5} = \frac{p_{5|0}}{p_{6|0}}\Delta_6 - \Delta_5, \quad \theta_{i,6} = \frac{1}{p_{6|0}\tau_{\text{des},i}}\Delta_6. \quad (11f)$$

In the absence of uncertainty (i.e.,  $\Delta = 0$ ), (11) reduces to the desired model (9).

Consider the CACC scheme for a heterogeneous platoon (i.e.,  $\tau_{\text{des},i} := \tau_i \neq \tau_{i-1}$ ) [3, 4]:

$$\begin{cases} \dot{\rho}_i = -\frac{1}{h_i}\rho_i + \frac{k_p}{h_i}e_i + \frac{k_d}{h_i}\dot{e}_i \\ \quad + \frac{\tau_{i-1} - \tau_i}{h_i\tau_{i-1}}a_{i-1} + \frac{\tau_i}{h_i\tau_{i-1}}u_{i-1}, \\ u_i = \rho_i, \end{cases} \quad (12)$$

where  $e_i := d_i - d_{r,i}$  denotes the spacing error, with inter-vehicle distance  $d_i = q_{i-1} - q_i - L_i$ , vehicle's length  $L_i$ , and control gains  $(k_p, k_d)$ . Define the follower and leader states  $x_i = [d_i \ v_i \ a_i]^\top$  and  $x_{i-1} = [v_{i-1} \ a_{i-1}]^\top$ , respectively. Substituting (12) into (11) yields the closed-

loop system

$$\begin{bmatrix} \dot{x}_{i-1} \\ \dot{x}_i \\ \dot{\rho}_i \end{bmatrix} = \begin{bmatrix} A_{i-1,i-1}^0 & 0 & 0 \\ A_{i,i-1}^0 & A_{i,i}^0 & B_{i,i}^0 \\ B_{i,i-1}^c & B_{i,i}^c & A_i^c \end{bmatrix} \begin{bmatrix} x_{i-1} \\ x_i \\ \rho_i \end{bmatrix} + [(B_{i-1}^0)^\top \ 0 \ (E_i^c)^\top]^\top u_{i-1} + [0 \ (B_i^\phi)^\top \ 0]^\top \phi_i, \quad (13)$$

where superscripts 0 and  $c$  indicate the nominal and controller matrices, respectively, given in Appendix A. The base controller (12) achieves the desired tracking performance for (9) (i.e.,  $\phi_i = \Delta = 0$ ). However, for the true closed-loop system (13), performance degradation occurs due to  $\phi_i$ .

To enhance robustness of (13) without altering the nominal closed-loop behavior, we exploit PEC realizations [18, 19], i.e., distinct realizations producing the same control input  $u_i$  in the nominal case while modifying the internal controller dynamics. To obtain the PEC realization of (12), define a new controller state  $\bar{\rho}_i$  via the linear transformation [18, 19]:

$$\bar{\rho}_i = \rho_i + F_{i,i}x_i + F_{i,i-1}x_{i-1}, \quad (14)$$

where  $F_{i,i} \in \mathbb{R}^{1 \times 3}$  and  $F_{i,i-1} \in \mathbb{R}^{1 \times 2}$ . To preserve the CACC information structure, explicit dependencies on vehicle  $i-2$  are excluded by omitting  $d_{i-1}$  in (14).

Differentiating (14) and substituting the nominal dynamics (9) and (12) yields the PEC realization

$$\begin{cases} \dot{\bar{\rho}}_i = \bar{A}_i^c \bar{\rho}_i + \bar{B}_{i,i}^c x_i + \bar{B}_{i,i-1}^c x_{i-1} + \bar{E}_i^c u_{i-1}, \\ u_i = \bar{\rho}_i - F_{i,i}x_i - F_{i,i-1}x_{i-1}, \end{cases} \quad (15a)$$

with

$$\bar{A}_i^c = A_i^c + F_{i,i}B_i^0, \quad \bar{E}_i^c = E_i^c + F_{i,i-1}B_{i-1}^0 \quad (15b)$$

$$\bar{B}_i^c = B_i^c + F_{i,i}A_{i,i}^0 - F_{i,i}B_{i,i}^0F_{i,i} - A_i^cF_{i,i}, \quad (15c)$$

$$\begin{aligned}\bar{B}_{i,i-1}^c = & B_{i,i-1}^c + F_{i,i-1}A_{i-1,i-1}^0 + F_{i,i}A_{i,i-1}^0 \\ & - F_{i,i}B_{i,i}^0F_{i,i-1} - A_i^cF_{i,i-1}.\end{aligned}\quad (15d)$$

While the base controller (12) guarantees nominal performance by design [3, 4], its internal realization is not unique which is observed in the PEC realization (15). This non-uniqueness can be exploited to improve robustness without altering the nominal behavior.

Therefore, the problem addressed in this paper is to determine a PEC realization that improves the robustness of a CACC-controlled vehicle in the presence of parametric uncertainty. Specifically, given the base controller (12), we seek a PEC realization of the form (15), by selecting the realization matrices  $F_{i,i}$  and  $F_{i,i-1}$ , such that the influence of the uncertainty  $\phi_i$  on (13) is minimized, aiming to preserve the nominal closed-loop behavior.

#### IV. Approach

This section derives the closed-loop dynamics under the PEC realization while accounting for parametric uncertainty. Throughout the analysis, we assume that the leader vehicle is free of uncertainty, i.e.,  $\phi_1 = 0$ . Without loss of generality, we restrict the problem to a

two-vehicle platoon  $S_m = \{1, 2\}$  and focus on the follower vehicle  $i = 2$ . This allows us to avoid cumbersome subscripts while preserving the structure of the problem. Accordingly, we drop the subscript  $i$  from  $F_{i,i}$  and  $F_{i,i-1}$  and define  $F := [F_2 \ F_1] = [f_{2,1}, f_{2,2}, f_{2,3}, f_{1,1}, f_{1,2}]$ . After deriving the closed-loop dynamics, we formulate an optimization problem using Lemmas 1 and 2 to derive the PEC realization that minimizes the impact of the parametric uncertainty  $\phi_2$  on the nominal closed-loop behavior.

### A. Uncertain Closed-Loop Dynamics

Substituting the PEC realization (15) into the uncertain dynamics (11) yields the closed-loop system

$$\begin{bmatrix} \dot{x}_1 \\ \dot{x}_2 \\ \dot{\rho}_2 \end{bmatrix} = \begin{bmatrix} A_{1,1}^0 & 0 & 0 \\ A_{2,1}^0 - B_2^0 F_1 & A_{2,2}^0 - B_2^0 F_2 & B_2^0 \\ \bar{B}_{2,1}^c & \bar{B}_{2,2}^c & \bar{A}_2^c \end{bmatrix} \begin{bmatrix} x_1 \\ x_2 \\ \bar{\rho}_2 \end{bmatrix} + \begin{bmatrix} (B_1^0)^\top & 0 & \bar{E}_2^c \end{bmatrix}^\top u_1 + \begin{bmatrix} 0 & (B_2^\phi)^\top & 0 \end{bmatrix}^\top \phi_2, \quad (16)$$

where the corresponding system matrices are given in Appendix A. By construction, the nominal closed-loop behavior of (16) is equivalent to that of (13), i.e., when  $\Delta = \phi_2 = 0$ . However, the choice of PEC realization matrix  $F$  affects the closed-loop behavior in the presence of parametric uncertainty, i.e., when  $\Delta \neq 0$  or, equivalently,  $\phi_2 \neq 0$ .

To explicitly characterize the influence of the PEC realization, we rewrite the closed-loop dynamics (16) in the original controller coordinates  $\rho_2$  by applying the inverse transformation of (14). In the case of uncertainties, this yields

$$\begin{bmatrix} \dot{x}_1 \\ \dot{x}_2 \\ \dot{\rho}_2 \end{bmatrix} = \begin{bmatrix} A_{1,1}^0 & 0 & 0 \\ A_{2,1}^0 & A_{2,2}^0 & B_{2,2}^0 \\ \bar{B}_{2,1}^c & \bar{B}_{2,2}^c & \bar{A}_2^c \end{bmatrix} \begin{bmatrix} x_1 \\ x_2 \\ \bar{\rho}_2 \end{bmatrix} + \begin{bmatrix} B_1^0 \\ 0 \\ \bar{E}_2^c \end{bmatrix} u_1 + \begin{bmatrix} 0 & (B_2^\phi)^\top & -F_2 B_2^\phi \end{bmatrix}^\top \phi_2. \quad (17)$$

From (17), it is evident that the PEC realizations only affect the mapping of the uncertainty  $\phi_2$  into the closed-loop dynamics. Moreover, this dependence occurs through the product  $F_2 B_2^\phi$ , which reduces to the scalar parameter  $f_{2,3}$ . Consequently, although  $F \in \mathbb{R}^{1 \times 5}$ , the effect of the PEC realization with respect to parametric uncertainty is fully characterized by the parameter  $f_{2,3}$ .

Since this result holds without imposing any assumptions on the structure of  $\phi_2$ , the remaining PEC parameters can be fixed without affecting robustness. In particular, inspired by [4], we choose  $f_{1,2} = -\frac{\tau_i}{h_i}$ , which yields PEC realizations that are independent of the leader input  $u_1$  (i.e.,  $\bar{E}_2^c = 0$ ) and driveline time constant  $\tau_{i-1}$ . The latter property is especially relevant for heterogeneous platoons, as it avoids dependency on the driveline dynamics of the preceding vehicle.

To determine  $f_{2,3}$ , we use Lemma 1 and Lemma 2, corresponding to Quadratic Stability and the Bounded-Real Lemma for polytopic uncertain systems, respectively. To this end, the nonlinear uncertainty  $\phi_2$  is approximated by

a first-order Taylor expansion around an operating point  $(v_i^*, a_i^*, u_i^*)$ . We assume that both the leader and the follower vehicle travel at a constant reference velocity  $v_r$ , yielding  $(v_i^*, a_i^*, u_i^*) = (v_r, 0, 0)$ . Under this assumption, the closed-loop dynamics (17) reduce to:

$$\begin{bmatrix} \dot{x}_1 \\ \dot{x}_2 \\ \dot{\rho}_2 \end{bmatrix} = \left( \begin{bmatrix} A_{1,1}^0 & 0 & 0 \\ A_{2,1}^0 & A_{2,2}^0 & B_{2,2}^0 \\ \bar{B}_{2,1}^c & \bar{B}_{2,2}^c & \bar{A}_2^c \end{bmatrix} + \begin{bmatrix} 0 & 0 & 0 \\ 0 & A_2^\Delta & B_2^\Delta \\ 0 & -F_2 A_2^\Delta & -F_2 B_2^\Delta \end{bmatrix} \right) \begin{bmatrix} x_1 \\ x_2 \\ \rho_2 \end{bmatrix} + \begin{bmatrix} B_1^0 \\ 0 \\ 0 \end{bmatrix} u_1 + \begin{bmatrix} (B_0^0)^\top & -F_2 B_0^0 \end{bmatrix}^\top \quad (18a)$$

where substitution of (11c)–(11f) yields

$$A_2^\Delta = \sum_{j=1}^6 A_{2,j}^\Delta \Delta_j, \quad B_2^\Delta = \sum_{j=1}^6 B_{2,j}^\Delta \Delta_j, \quad B_0^\Delta = \sum_{j=1}^6 B_{0,j}^\Delta \Delta_j. \quad (18b)$$

The matrices  $A_{2,j}^\Delta, B_{2,j}^\Delta, B_{0,j}^\Delta$  are given in Appendix B.

Define the uncertainty vector

$$\Delta := [\Delta_1 \ \Delta_2 \ \Delta_3 \ \Delta_4 \ \Delta_5 \ \Delta_6]^\top, \quad (19)$$

and the corresponding hyper-rectangle uncertainty set

$$\Delta \in \mathcal{D} := \{\Delta \in \mathbb{R}^6 : \Delta_j \in [\underline{\Delta}_j, \bar{\Delta}_j], j \in \{1, \dots, 6\}\}. \quad (20)$$

Since  $A_2^\Delta, B_2^\Delta$ , and  $B_0^\Delta$  depend affinely on  $\Delta_j$ , their image over  $\mathcal{D}$  lies in the convex hull of the matrices evaluated at the vertices of  $\mathcal{D}$ . There are  $2^6$  vertices, corresponding to all binary combinations of lower and upper bounds. For each vertex  $k = 1, \dots, 2^6$ , let  $v^{[k]} \in \{0, 1\}^6$  indicate whether to use the lower ( $v_j^{[k]} = 0$ ) or upper ( $v_j^{[k]} = 1$ ) bound. Then

$$\Delta^{[k]} = (1 - v_j^{[k]}) \Delta_j + v_j^{[k]} \bar{\Delta}_j, \quad (21a)$$

$$A_2^{\Delta^{[k]}} = \sum_{j=1}^6 A_{2,j}^\Delta \Delta_j^{[k]}, \quad B_2^{\Delta^{[k]}} = \sum_{j=1}^6 B_{2,j}^\Delta \Delta_j^{[k]}, \quad (21b)$$

$$B_0^{\Delta^{[k]}} = \sum_{j=1}^6 B_{0,j}^\Delta \Delta_j^{[k]}, \quad \forall k \in \{1, \dots, 2^6\}. \quad (21c)$$

Consequently, for any  $\Delta \in \mathcal{D}$ , the uncertain matrices belong to the polytope

$$A_2^\Delta = \sum_{k=1}^{2^6} \sum_{j=1}^6 \beta_k A_{2,j}^\Delta \Delta_j^{[k]}, \quad B_2^\Delta = \sum_{k=1}^{2^6} \sum_{j=1}^6 \beta_k B_{2,j}^\Delta \Delta_j^{[k]}, \quad (22a)$$

$$B_0^\Delta = \sum_{k=1}^{2^p} \sum_{j=1}^p \beta_k B_{0,j}^\Delta \Delta_j^{[k]}, \quad \sum_{k=1}^{2^6} \beta_k = 1, \quad \beta_k \geq 0. \quad (22b)$$

Closed-loop system (18) together with (22) constitutes a polytopic uncertain system (Definition 1), which allows the use of Lemmas 1 and 2 to compute the optimal value of  $f_{2,3}$ .

### B. Optimal PEC Realization

The objective is to derive the optimal PEC realization, i.e., the optimal value of  $f_{2,3}$ , such that the effect of the

parametric uncertainty  $\Delta$  on the closed-loop behavior is minimized. To this end, we employ Lemmas 1 and 2, both of which require the system matrix  $A$  to be Hurwitz. However, in (18),  $A_{1,1}^0$  is not Hurwitz due to the uncontrolled leader, which introduces an integrator associated with the leader velocity. To circumvent this issue, the leader state  $x_1$  is treated as an exogenous input, and the stability and performance analysis is restricted to the follower.

Furthermore, the leader is assumed to track a constant reference velocity  $v_r$ , used as the operating point for linearizing  $\phi_2$ . This motivates the coordinate transformation  $\tilde{x}_1 := [\tilde{v}_1 \ a_1]^\top$ , with  $\tilde{v}_1 = v_1 - v_r$ , and we assume that  $\tilde{x}_1 \in \mathcal{L}_2$ .

Define the reduced closed-loop state  $\zeta := [x_2^\top \ \rho_2]^\top$ . Then, the closed-loop dynamics (18) can be written as

$$\dot{\zeta} = (\mathcal{A}^0 + \mathcal{A}^\Delta)\zeta + \mathcal{B}_1^0 \tilde{x}_1 + \mathcal{B}_0^\Delta, \quad (23a)$$

$$\mathcal{A}^0 = \begin{bmatrix} A_{2,2}^0 & B_2^0 \\ B_2^c & A_2^c \end{bmatrix}, \quad \mathcal{A}^\Delta = \begin{bmatrix} A_2^\Delta & B_2^\Delta \\ -F_2 A_2^\Delta & -F_2 B_2^\Delta \end{bmatrix}, \quad (23b)$$

$$\mathcal{B}_1^0 = [(A_{2,1}^0)^\top \ B_{2,1}^c]^\top, \quad \mathcal{B}_0^\Delta = [(B_0^\Delta)^\top \ -F_2 B_0^\Delta]^\top. \quad (23c)$$

The goal is to find  $f_{2,3}$ , embedded in  $F_2$ , to minimize the deviation of the uncertain closed-loop system (23) from the desired nominal behavior. To quantify the deviation induced by the uncertainty, we introduce the nominal model

$$\dot{\zeta}^0 = \mathcal{A}^0 \zeta^0 + \mathcal{B}_1^0 \tilde{x}_1. \quad (24)$$

For  $\Delta = 0$ , (23) reduces to (24). Using the nominal model, we define the closed-loop error state  $\zeta^e := \zeta - \zeta^0$ . Subtracting the nominal dynamics (24) from (23) yields the dynamics

$$\dot{\zeta}_e = (\mathcal{A}^0 + \mathcal{A}^\Delta)\zeta_e + \mathcal{A}^\Delta \zeta_0 + \mathcal{B}_0^\Delta. \quad (25)$$

Next, we define the stacked state  $q := [\zeta_0^\top \ \zeta_e^\top]^\top$ , which evolves according to

$$\dot{q} = \underbrace{\begin{bmatrix} \mathcal{A}^0 & 0 \\ \mathcal{A}^\Delta & \mathcal{A}^0 + \mathcal{A}^\Delta \end{bmatrix}}_{\mathcal{A}_q} q + \underbrace{\begin{bmatrix} \mathcal{B}_1^0 \\ 0 \end{bmatrix}}_{\mathcal{B}_q} \tilde{x}_1 + \begin{bmatrix} 0 \\ \mathcal{B}_0^\Delta \end{bmatrix}. \quad (26)$$

This augmented system captures both the nominal closed-loop dynamics, represented by  $\zeta^0$ , and the deviation induced by the parametric uncertainty, represented by the error state  $\zeta^e$ . Since the uncertainty enters the dynamics through  $\mathcal{A}^\Delta$ , which depends linearly on  $F_2$  (i.e.,  $f_{2,3}$ ), the system (26) provides a suitable framework for quantifying and minimizing the impact of the parametric uncertainty  $\Delta$  in platooning.

The design objective is twofold. First, we seek to reduce the influence of the nominal state  $\zeta^0$  on the error state  $\zeta^e$ . This is achieved by minimizing  $\text{trace}(C_z P C_z^\top)$  in Lemma 2, thereby reducing the average energy of  $\zeta^e$  in the output [21]. Second, since accurate tracking of the leader is a primary control objective of CACC, we aim to reduce the effect of the leader state  $\tilde{x}_1$  on error  $\zeta^e$ .

This motivates minimizing the worst-case amplification of  $\tilde{x}_1$  to  $\zeta^e$ , hence minimizing  $\gamma$  in Lemma 2.

To achieve this objective, we define the performance output  $z$  as the error state

$$z := [0 \ C] q = C_z q, \quad (27a)$$

$$C = \text{diag}([1, 1, 1, 0]), \quad (27b)$$

hence we solely focus on the vehicle states  $x_2$  and not the controller state  $\rho_2$ . Consider the polytopic uncertain closed-loop system (22), (23), (26), performance output (27), and uncertainty (20). Based on Lemmas 1 and 2, for a given  $f_{2,3}$ , if there exist a positive definite matrix  $P \in \mathbb{R}^{8 \times 8}$  and a scalar  $\gamma > 0$ , being the solution to the convex program:

$$\begin{cases} \min_{P, \gamma} & \text{trace}(C_z P C_z^\top) + \gamma, \\ \text{s.t.} & (\mathcal{A}_q)^\top P + P \mathcal{A}_q \prec 0, \quad k = 1, \dots, 2^6, \\ & \begin{bmatrix} (\mathcal{A}_q)^\top P + P \mathcal{A}_q + C_z^\top C_z & P \mathcal{B}_q \\ (\mathcal{B}_q)^\top P & -\gamma I \end{bmatrix} \preceq 0, \end{cases} \quad (28)$$

then the optimal value  $f_{2,3}^*$  stabilizes the uncertain system while minimizing both the average output energy and worst-case amplification with respect to the leader states. This objective function reflects a trade-off between reducing error dynamic energy and suppressing leader-induced deviations, which is further discussed in the results section.

Note that (28) is solved via a line-search over  $f_{2,3}$ , as then the formulation reduces to an LMI. Future work will investigate reformulating the LMI to solve for  $F_2$  directly, avoiding intensive grid searches as design degrees of freedom increase. The proposed optimization framework is experimentally validated, and the results are discussed in the subsequent section.

## V. Case Study Results

This section presents the results obtained by solving the optimization problem (28). The objective of (28) is to enhance the robustness of the uncertain closed-loop system (13) with respect to  $\phi_2$ , i.e.,  $\Delta$ , while preserving the desired closed-loop behavior. Both the simulation study and the experimental validation are conducted using the vehicle parameters and associated uncertainties listed in TABLE I. The optimization problem is solved in MATLAB 2025b using YALMIP [22], with solver MOSEK [23].

We consider six different realizations, denoted by  $F^l$ ,  $l \in \{0, \dots, 5\}$ , where  $F^0$  corresponds to the base controller. The optimization problem is solved for a range of operating points  $v_r \in [0, 100]$  km/h. Although the optimal cost increases with  $v_r$ , the optimizer  $f_{2,3}^*$  remains unchanged. Consequently, all results in the remainder of this section are solved for  $v_r = 50$  km/h.

The resulting controller realization matrices are summarized in TABLE II. Realization  $F^1$  modifies all realization entries except for  $f_{2,3}$ , which, according to Section IV-A, should yield identical closed-loop behavior to the base realization  $F^0$  in the presence of uncertainty.

TABLE I

Vehicle Parameters and estimated uncertainties of the Renault Twizy test platform.

Sym.	Parameter	Nominal	Range ( $\Delta$ )	Unit
$m$	Vehicle Mass	731	[716, 746]	kg
$m_{\text{eff}}$	Effective Mass	778	[763, 793]	kg
$f_v$	Viscous Friction	5.55	[5.5, 5.6]	Ns/m
$f_r$	Rolling Res. Coeff.	0.0262	[0.0262, 0.0262]	–
$C_d$	Aero. Drag Factor	0.392	[0.3528, 0.4312]	kg/m
$\tau$	Time Constant	0.12	[0.11, 0.13]	s
$\alpha$	Road Slope	0	[0, 0]	rad
$v_w$	Wind Velocity	0	[-5, 5]	m/s
$k_p$	Proportional gain	0.2	–	1/s <sup>2</sup>
$k_d$	Derivative gain	0.7	–	1/s
$h$	Headway time	0.2	–	s
$r$	Standstill distance	0	–	m

TABLE II

Controller Realizations for Case Study Results.

Objective	$\mathbf{F}$
$F_0$ Base controller	$[0, 0, 0, 0, -\frac{\tau_i}{h_i}]$
$F_1$ Equal performance	$[-\frac{\tau_i}{h_i}, -\frac{\tau_i}{h_i}, 0, -\frac{\tau_i}{h_i}, -\frac{\tau_i}{h_i}]$
$F_2$ Poor performance	$[0, 0, 0.3, 0, -\frac{\tau_i}{h_i}]$
$F_3$ Minimal trace( $C_z P C_z^\top$ ) + $\gamma$	$[0, 0, 0.14865, 0, -\frac{\tau_i}{h_i}]$
$F_4$ Minimal trace( $C_z P C_z^\top$ )	$[0, 0, 0.15866, 0, -\frac{\tau_i}{h_i}]$
$F_5$ Minimal $\gamma$	$[0, 0, 0.11662, 0, -\frac{\tau_i}{h_i}]$

Realizations  $F^3$ ,  $F^4$ , and  $F^5$  are obtained by solving (28) with different objective functions. Since (28) jointly minimizes trace( $C_z P C_z^\top$ ) and  $\gamma$ , the optimization problem is also solved for each objective individually to isolate their respective effects. Finally, a deliberately suboptimal realization  $F^2$  is included to verify whether degraded performance is observed.

### A. Simulation Results

The controller realizations in TABLE II are evaluated in a MATLAB simulation of a two-vehicle platoon, consisting of a leader ( $i = 1$ ) and a follower ( $i = 2$ ). Model mismatch is introduced in the follower vehicle by setting all parameters at their lower bounds (TABLE I), together with a constant wind velocity  $v_w = 15$  km/h. The leader tracks a reference velocity  $v_r = 15$  km/h and applies the following step input:

$$u_1(t) = \begin{cases} 1 & 10 \leq t \leq 11, \\ -1 & 21 \leq t \leq 22, \\ 0 & \text{otherwise.} \end{cases} \quad (29)$$

The resulting follower velocity and spacing error are shown in Fig. 2 for each realization  $F^l$ ,  $l \in \{1, \dots, 5\}$ . For reference, the nominal response (i.e.,  $\Delta = 0$ ) is included and is indicated by the solid black line.

To quantify the deviation between the uncertain and nominal closed-loop behavior, the root-mean-square error (RMSE) between  $\zeta^0$  and  $\zeta$  is reported in TABLE III. Although the visual differences in Fig. 2 are subtle, the RMS values clearly demonstrate the superior performance of realization  $F^5$ . In contrast, the anticipated benefits of realization  $F^4$  are not observed. While the objective trace( $C_z P C_z^\top$ ) targets transient deviations

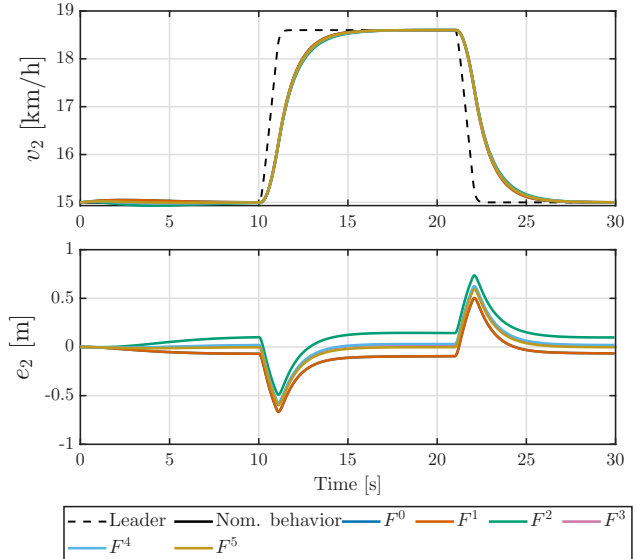


Fig. 2. Time-domain simulation of a two-vehicle CACC platoon with parameters from TABLE I subject to parameter mismatch (uncertainties at lower bounds, positive wind velocity). Follower velocity  $v_2$  and spacing error  $e_2$  are shown for the controller realizations in TABLE II.

TABLE III  
Comparison of Velocity RMSE and Spacing RMSE

Realization	Velocity RMSE	Spacing RMSE
$F^0$	0.0238 (–)	0.1554 (–%)
$F^1$	0.0238 (–0%)	0.1554 (–0%)
$F^2$	0.0318 (+34%)	0.2082 (+33%)
$F^3$	0.0186 (–23%)	0.1550 (–0.3%)
$F^4$	0.0191 (–20%)	0.1571 (+1%)
$F^5$	0.0179 (–25%)	0.1498 (–4%)

between  $\zeta^0$  and  $\zeta^e$ , these effects are negligible in the present scenario. As a result, minimizing  $\gamma$  dominates the performance, rendering trace( $C_z P C_z^\top$ ) ineffective as an objective in this case. The degraded performance of the suboptimal realization  $F^2$  is clearly visible, while  $F^1$  reproduces the behavior of the base controller  $F^0$ , as expected.

### B. Experimental Results

The proposed controller realizations in TABLE II are validated experimentally on the Renault Twizy test platform in Fig. 3, an electric vehicle equipped with a real-time computer for autonomous operation. Details on the vehicle hardware and software are provided in [5]. The vehicle parameters and estimated uncertainty are listed in TABLE I. To complement the simulation study, an equivalent platooning scenario is implemented experimentally. A virtual leader is simulated on the follower vehicle's real-time computer to enforce nominal leader dynamics. The virtual leader evolves according to the desired dynamics (9), with  $\tau_{i-1} = 0.12$  s, tracks a reference velocity of  $v_r = 15$  km/h, and applies the step input defined in (29). Inter-vehicle distance is obtained by integrating the relative velocity. Experimental results are shown in Fig. 4. Transients at the start and end of the trajectory arise from cornering maneuvers required due to spatial constraints.



Fig. 3. Renault Twizy experimental vehicle, details are provided in [5].

Overall, the experimental results align with the simulation study. In particular, the equivalence between realizations  $F^0$  and  $F^1$  is confirmed, as both yield nearly identical responses. The degraded performance of the suboptimal realization  $F^2$  is clearly observable. Differences between realizations  $F^3$ ,  $F^4$ , and  $F^5$  are more subtle; nevertheless, realization  $F^5$  exhibits the best overall performance, characterized by the smallest steady-state velocity error.

A subsequent experiment at  $v_r = 50$  km/h is performed, where  $F^1$  and  $F^2$  were omitted due to the established equivalence of  $F^1$  with  $F^0$  and the poor performance of  $F^2$ . The results in Fig. 5 indicate that the vehicle is less affected by the model uncertainty at higher velocities, yielding similar responses across all tested realizations. This suggests that the nominal parameters align more closely with the true dynamics at this reference velocity, thereby reducing the model mismatch. Given that the parameter identification in Table I was obtained experimentally, the resulting nominal model is likely biased toward the higher-velocity data sets used during identification, potentially failing to represent low speeds sufficiently. The fact that all realizations yield similar responses in this test is not a limitation of the proposed method, but rather a positive. Since the system identification is velocity-dependent, it inherently introduces model mismatch across different velocities. The optimized PEC realizations provide the necessary robustness to compensate for this mismatch where it occurs (e.g., at low speeds), while exhibiting nominal behavior when the nominal parameters align with the true parameters.

Furthermore, although the overall conclusion remains the same, the experimental responses exhibit noticeably larger deviations from the leader than observed in the simulation. This discrepancy is likely due to unmodeled actuation delay. Including such delays in the simulation produces responses that better match the experimental data, as shown in Fig. 6. Simulations indicate that actuation delay can reduce the benefits of optimized controller realizations relative to the base controller.

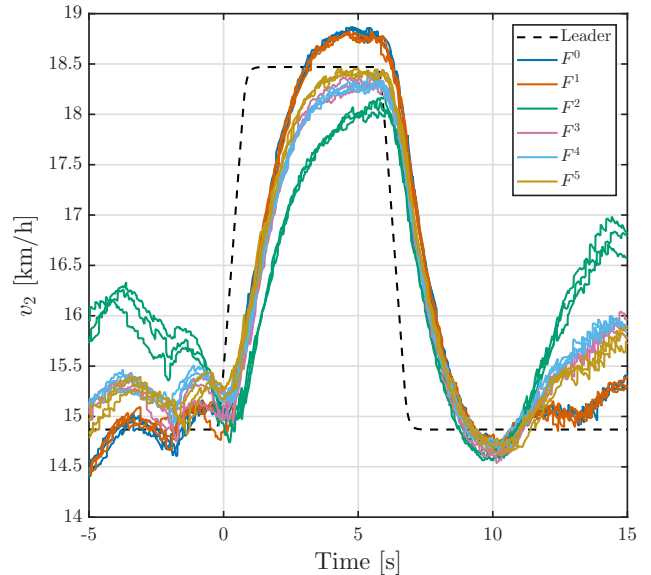


Fig. 4. Experimental response of a Renault Twizy characterized by the parameters in TABLE I, tracking a virtual leader at 15 km/h. Follower velocity  $v_2$  is shown for the realizations in TABLE II.

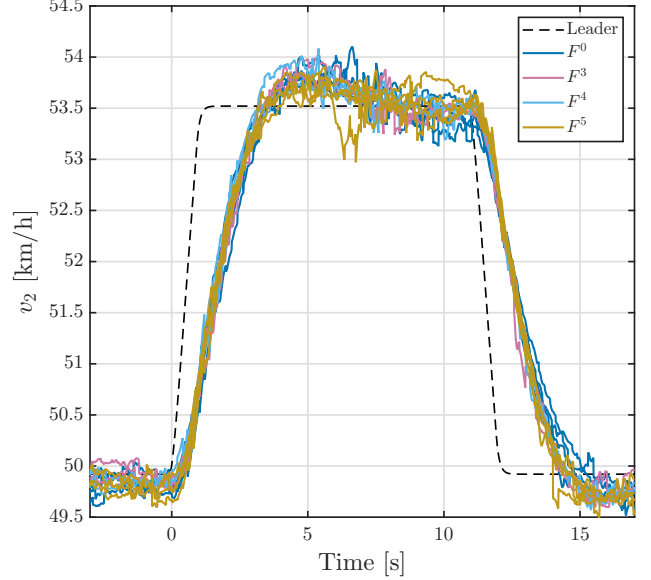


Fig. 5. Experimental response of a Renault Twizy characterized by the parameters in TABLE I, tracking a virtual leader at 50 km/h. Follower velocity  $v_2$  is shown for the realizations in TABLE II.

Explicitly accounting for actuation delay in the PEC realizations, e.g., via a Padé approximation as in [5], may enable further performance improvements.

## VI. CONCLUSIONS AND FUTURE WORKS

This paper proposes a robustness-enhancing CACC framework based on plant-equivalent controller realizations. By exploiting alternative controller realizations that preserve the nominal control input, robustness against parametric uncertainty is improved without altering the nominal closed-loop behavior. Robust stability and performance are enforced using LMI-based conditions, and experimental results demonstrate the effectiveness of the proposed approach.

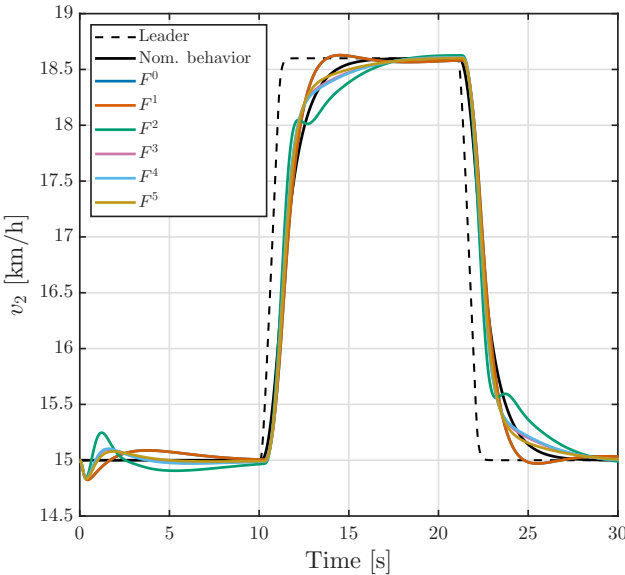


Fig. 6. Time-domain simulation of a two-vehicle CACC platoon with parameters from TABLE I subject to parameter mismatch (uncertainties at lower bounds, positive wind velocity) and 0.2 s actuation delay. Follower velocity  $v_2$  is shown for the controller realizations in TABLE II.

Future work will focus on extending the framework to include actuation delay and on reformulating the LMI conditions to solve for  $F_2$  directly, thereby avoiding grid searches as the number of design degrees of freedom increases.

## VII. ACKNOWLEDGMENTS

The authors would like to express their gratitude to Redmer de Haan for his supervision and the valuable discussions regarding the experiments.

## References

- [1] J. Guanetti et al., "Control of connected and automated vehicles: State of the art and future challenges," *Annual Reviews in Control*, vol. 45, pp. 18–40, 2018.
- [2] A. Ghasemi et al., "Stable Decentralized Control of a Platoon of Vehicles With Heterogeneous Information Feedback," *IEEE Transactions on Vehicular Technology*, vol. 62, pp. 4299–4308, 2013.
- [3] J. Ploeg et al., "Design and experimental evaluation of cooperative adaptive cruise control," in 2011 14th International IEEE Conference on Intelligent Transportation Systems (ITSC), IEEE, 2011, pp. 260–265.
- [4] E. Lefeber et al., "Cooperative Adaptive Cruise Control of Heterogeneous Vehicle Platoons," *IFAC-PapersOnLine*, vol. 53, pp. 15 217–15 222, 2020.
- [5] R. De Haan et al., "Cooperative Adaptive Cruise Control for Heterogeneous Platoons With Delays: Controller Design and Experiments," *IEEE Transactions on Control Systems Technology*, vol. 33, pp. 1361–1371, 2025.
- [6] P. Wijnbergen and B. Besselink, "Existence of decentralized controllers for vehicle platoons: On the role of spacing policies and available measurements," *Systems & Control Letters*, vol. 145, p. 104 796, 2020.
- [7] S. Baldi et al., "Establishing Platoons of Bidirectional Cooperative Vehicles With Engine Limits and Uncertain Dynamics," *IEEE Transactions on Intelligent Transportation Systems*, vol. 22, pp. 2679–2691, 2021.
- [8] F. Gao et al., "Robust control of heterogeneous vehicular platoon with uncertain dynamics and communication delay," *IET Intelligent Transport Systems*, vol. 10, pp. 503–513, 2016.
- [9] S. E. Li et al., "Robust Longitudinal Control of Multi-Vehicle Systems—A Distributed H-Infinity Method," *IEEE Transactions on Intelligent Transportation Systems*, vol. 19, pp. 2779–2788, 2018.
- [10] Y. Zhu et al., "Adaptive Optimal Control of Heterogeneous CACC System With Uncertain Dynamics," *IEEE Transactions on Control Systems Technology*, vol. 27, pp. 1772–1779, 2019.
- [11] Y. S. Quan et al., "Robust Adaptive Cruise Control Design Using Model Predictive Control," *IEEE Transactions on Intelligent Vehicles*, pp. 1–10, 2024.
- [12] X. Yang et al., "Adaptive Controller Design for Heterogeneous Cooperative Adaptive Cruise Control System with Uncertain Vehicle Parameters," in 2023 IEEE 26th International Conference on Intelligent Transportation Systems (ITSC), IEEE, 2023, pp. 3712–3716.
- [13] H. Xing et al., "Robust CACC in the Presence of Uncertain Delays," *IEEE Transactions on Vehicular Technology*, vol. 71, pp. 3507–3518, 2022.
- [14] A. Alam et al., "Guaranteeing safety for heavy duty vehicle platooning: Safe set computations and experimental evaluations," *Control Engineering Practice*, vol. 24, pp. 33–41, 2014.
- [15] S. Sheikholeslam and C. Desoer, "Longitudinal control of a platoon of vehicles with no communication of lead vehicle information: A system level study," *IEEE Transactions on Vehicular Technology*, vol. 42, pp. 546–554, 1993.
- [16] P. Sahlholm and K. Henrik Johansson, "Road grade estimation for look-ahead vehicle control using multiple measurement runs," *Control Engineering Practice*, vol. 18, pp. 1328–1341, 2010.
- [17] B. Besselink et al., "Cyber-Physical Control of Road Freight Transport," *Proceedings of the IEEE*, vol. 104, pp. 1128–1141, 2016.
- [18] M. Huisman et al., "Optimal Controller Realizations against False Data Injections in Cooperative Driving," in 2024 IEEE 63rd Conference

on Decision and Control (CDC), IEEE, 2024, pp. 2349–2354.

[19] M. Huisman et al., “Plant Equivalent Controller Realizations for Attack-Resilient Cyber-Physical Systems,” 2025.

[20] S. X. Ding, Model-Based Fault Diagnosis Techniques: Design Schemes, Algorithms and Tools (Advances in Industrial Control). Springer London, 2013.

[21] S. P. Boyd, Ed., Linear matrix inequalities in system and control theory (SIAM studies in applied mathematics). Society for Industrial and Applied Mathematics, 1994.

[22] J. Lofberg, “YALMIP : A toolbox for modeling and optimization in MATLAB,” in 2004 IEEE International Conference on Robotics and Automation (IEEE Cat. No.04CH37508), IEEE, 2004, pp. 284–289.

[23] M. ApS, The MOSEK optimization toolbox for MATLAB manual. Version 10.1. 2024.

## Appendix

### A. Nominal System Matrices

This appendix provides the nominal matrices for (13).

$$A_{i-1,i-1}^0 = \begin{bmatrix} 0 & -\frac{1}{\tau_{i-1}} \\ 0 & 0 \end{bmatrix}, A_{i,i-1}^0 = \begin{bmatrix} 1 & 0 \\ 0 & 0 \end{bmatrix}, B_{i-1}^0 = \begin{bmatrix} 0 \\ \frac{1}{\tau_{i-1}} \end{bmatrix}, \quad (30a)$$

$$A_{i,i}^0 = \begin{bmatrix} 0 & -1 & 0 \\ 0 & 0 & 1 \\ 0 & 0 & -\frac{1}{\tau_i} \end{bmatrix}, B_i^0 = \begin{bmatrix} 0 \\ 0 \\ \frac{1}{\tau_i} \end{bmatrix}, B_i^\phi = \begin{bmatrix} 0 \\ 0 \\ 1 \end{bmatrix}, \quad (30b)$$

$$A_i^c = -\frac{1}{h_i}, \quad B_{i,i-1}^c = \begin{bmatrix} \frac{k_d}{h_i} + \frac{\tau_{i-1} - \tau_i}{h_i \tau_{i-1}} & 0 \end{bmatrix}, \quad (30c)$$

$$B_{i,i}^c = \begin{bmatrix} \frac{k_p}{h_i} & -\left(k_p + \frac{k_d}{h_i}\right) & -k_d \end{bmatrix}, E^c = \frac{\tau_i}{h_i \tau_{i-1}}, \quad (30d)$$

### B. Uncertainty Matrices

This appendix provides the uncertainty matrices for (18).

$$A_{2,1}^\Delta = \begin{bmatrix} 0 & 0 & 0 \\ 0 & 0 & 0 \\ 0 & -1 & 0 \end{bmatrix}, A_{2,2}^\Delta = \begin{bmatrix} 0 & 0 & 0 \\ 0 & 0 & 0 \\ 0 & 0 & -1 \end{bmatrix}, \quad (31a)$$

$$A_{2,3}^\Delta = \begin{bmatrix} 0 & 0 & 0 \\ 0 & 0 & 0 \\ 0 & -2v_r & 0 \end{bmatrix}, A_{2,4}^\Delta = \begin{bmatrix} 0 & 0 & 0 \\ 0 & 0 & 0 \\ 0 & 0 & -v_r \end{bmatrix}, \quad (31b)$$

$$A_{2,6}^\Delta = \begin{bmatrix} 0 & 0 & 0 \\ 0 & 0 & 0 \\ 0 & \frac{p_{1|0} + 2p_{3|0}v_r}{p_{6|0}} & \frac{p_{2|0} + p_{4|0}v_r}{p_{6|0}} - \frac{1}{p_{6|0}\tau_{des}} \end{bmatrix}, \quad (31c)$$

$$B_{2,6}^\Delta = \begin{bmatrix} 0 \\ 0 \\ \frac{1}{p_{6|0}\tau_{des}} \end{bmatrix}, B_{0,3}^\Delta = \begin{bmatrix} 0 \\ 0 \\ v_r^2 \end{bmatrix}, B_{0,5}^\Delta = \begin{bmatrix} 0 \\ 0 \\ -1 \end{bmatrix}, \quad (31d)$$

$$B_{0,6}^\Delta = \begin{bmatrix} 0 & 0 & \frac{p_{5|0} - p_{3|0}v_r^2}{p_{6|0}} \end{bmatrix}^\top. \quad (31e)$$